BB

GSI

GSI-Preprint-95-75
NOVEMBER 1995

INTERACTION CROSS-SECTIONS AND MATTER RADII OF A = 20 ISOBARS

L. CHULKOV, G. KRAUS, O. BOCHKAREV, P. EGELHOF, H. GEISSEL, M. GOLOVKOV, H. IRNICH, Z. JANAS, H. KELLER, T. KOBAYASHI, G. MÜNZENBERG, F. NICKEL,A. OGLOBLIN, A. OZAWA, S. PATRA, A. PIECHACZEK, E. ROECKL, W. SCHWAB,K. SÜMMERER, T. SUZUKI, I. TANIHATA, K. YOSHIDA

SW9605

(Submitted to Nucl. Phys. A)

Gesellschaft für Schwerionenforschung mbH
Postfach 110552 · D-64220 Darmstadt Germany

Interaction cross-sections and matter radii of $A = 20$ isobars

L. Chulkov [a], G. Kraus [b], O. Bochkarev [a], P. Egelhof [b], H.Geissel [b], M. Golovkov [a], H. Irnich [b], Z. Janas [b], H. Keller [b], T. Kobayashi [c], G. Münzenberg [b], F. Nickel [b], A. Ogloblin [a], A. Ozawa [c], S. Patra [d], A. Piechaczek [b], E. Roeckl [b], W. Schwab [b], K. Sümmerer [b], T. Suzuki [c], I. Tanihata [c] and K. Yoshida [c]

[a] *Kurchatov Institute, Moscow, Russia*

[b] *GSI Darmstadt, Germany*

[c] *RIKEN, Saitama, Japan*

[d] *Physical Institute, Bhubaneswar, India*

Abstract

High-energy interaction cross-sections of $A = 20$ nuclei (^{20}N, ^{20}O, ^{20}F, ^{20}Ne, ^{20}Na, ^{20}Mg) on carbon were measured with accuracies of $\approx 1\%$. The nuclear matter rms radii derived from the measured cross-sections show an irregular dependence on isospin projection. The largest difference in radii, which amounts to approximately 0.2 fm, has been obtained for the mirror nuclei ^{20}O and ^{20}Mg. The influence of nuclear deformation and binding energy on the radii is discussed. By evaluating the difference in rms radii of neutron and proton distributions, evidence has been found for the existence of a proton skin for ^{20}Mg and of a neutron skin for ^{20}N.

1 Introduction

Generalized moments of nuclear density distributions are basic characteristics of nuclei and reflect main features of nuclear structure. The measurement of root mean square (rms) matter radii of light neutron-rich nuclei, for example, lead to the discovery of extended neutron halos or neutron skins [1,2]. There is corresponding experimental evidence that the phenomenon of proton halos or proton skins is to be expected for very proton-rich nuclei even though such an effect is strongly suppressed by the Coulomb force. For example, the data obtained from high-energy proton elastic scattering on $A = 48$ isobars were interpreted by assuming that the rms matter radius $< r_m^2 >^{1/2}$ of ^{48}Ti, having two protons in excess to the closed sd-shell, is

larger than that of ^{48}Ca [3]. Indeed, as was shown later, the charge radii $< r_c^2 >^{1/2}$ of $^{44-50}$Ti are larger by about 0.1 fm than those of the corresponding calcium isobars (see, for example, the discussion in ref. [4]). The enhanced interaction cross-section for the ^{8}B nucleus [5] and the narrow longitudinal momentum distribution of ^{7}Be fragments from the ^{8}B - breakup [6] yielded evidence for the existence of a very extended proton distribution in ^{8}B. Recently an increase of matter radii on the proton-rich side of $A = 17$ isobars has been deduced from a measurement of high-energy interaction cross-sections [7]. The enhanced $< r_m^2 >^{1/2}$ for ^{17}Ne was also explained by a specific shell structure of this nucleus [8]. The ^{20}Mg nucleus, consisting of a very tight ^{16}O core and four weakly bound protons above the closed p - shell, is a good candidate for the search for a proton skin as well.

Several methods exist to determine the radial parameters of nuclear matter density distributions and, in particular, the difference between proton and neutron distributions in nuclei: α - scattering at moderate energy, high-energy proton scattering, (π^-, π^-) - and (π^+, π^+) - scattering, and, finally, the measurement of high-energy nucleus-nucleus interaction cross-sections σ_I. All these methods have nearly the same sensitivity and give noncontradictory results (see, for example, refs. [9,10]). However, only the last one can be used in the case of nuclei very far from the beta stability line, where the intensities of secondary beams are limited to a few ions per second.

Nuclear matter radii are influenced by many factors, e.g. binding energy [11,12], odd-even staggering [13], zero-point motions of the surface [14], shell closure effects and deformation [15,16]. Therefore, comprehensive studies of a wide range of nuclei are necessary to draw definite conclusions. Such measurements can be performed by using intermediate energy or relativistic heavy-ion reactions, which give access to exotic nuclei within a wide range of the N/Z ratio. The aim of the experiment described here was the investigation of σ_I and of matter radii for a chain of $A = 20$ isobars.

We will show in this paper that σ_I mainly depends upon the rms radius of the matter distribution and is only slightly affected by the difference in neutron and proton radii and by the shape of the density distribution. Based on these arguments, rms matter radii can be obtained from the measured values of σ_I. It is clear that the changes of rms radii within an isobaric sequence are of special interest. However, changes in the $< r_m^2 >^{1/2}$ are not necessarily accompanied by a neutron or proton excess at the nuclear surface. We shall determine the differences in neutron and proton distributions by comparing the rms matter radii, measured in this work, to the rms radii of the proton distributions $< r_p^2 >^{1/2}$ obtained either experimentally or via extrapolation of existing experimental data by using relativistic mean field theory (RMF) calculations.

2 Experimental setup

Secondary beams of ^{20}N, ^{20}O, ^{20}F, ^{20}Ne, ^{20}Na and ^{20}Mg were produced at the GSI Fragment Separator FRS [18]. ^{36}Ar and ^{40}Ar beams with intensities of up to 2×10^9 ions per second were accelerated to 1050 A·MeV by the heavy ion synchrotron SIS and then fragmented in ^{9}Be production targets of 4 g/cm^2 and 1 g/cm^2. The σ_I of $A = 20$ nuclei on carbon were determined by a transmission-type measurement. For this purpose, different carbon targets with thicknesses of 7.5 and 3.7 g/cm^2 were placed at the intermediate focal plane F2 of the FRS. The homogeneity in thickness of these targets was better than 0.01%. The reaction products were isotopically identified in the first stage of the FRS (upstream from the target positioned at F2), as well as in the second stage of the FRS (downstream from the F2 target) with a ΔE - TOF - Bρ method, respectively. By using this method, the ratio of incoming and transmitted (non-reacting) particles was determined for each well-defined isotope. From this ratio the desired σ_I values were obtained.

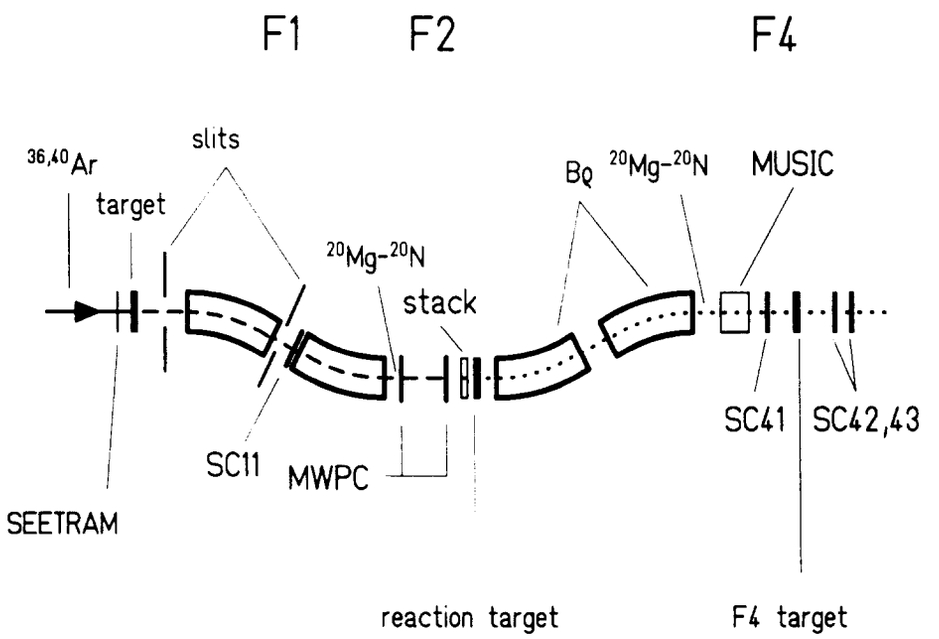

Fig. 1.

Experimental setup for the measurement of interaction cross-sections of $A = 20$ nuclei by using the transmission method.

The experimental setup, which was also used for determining σ_I values of a chain of sodium isotopes [17], is shown in Fig. 1. Besides the magnetic rigidity ($B\rho$) anal-

ysis of secondary beams in the FRS and slits for suppression of unwanted isotopes, several detectors have been used for the reaction product identification upstream and downstream from the F2 target. The nuclear charge Z was derived from energy deposition (ΔE) measurements performed by using a stack of five 3 mm thick plastic scintillators at F2 and a multisampling ionization chamber (MUSIC) at the focal plane F4. For determination of the nuclear mass A, the time of flight (TOF) for each fragment was measured between F1 and F2 (18 m) as well as between F2 and F4 (36 m), using fast plastic scintillators which are denoted by SC11, stack and SC41 in Fig. 1. In both sections of the FRS, i.e. upstream and downstream from F2, the Δ E resolution of $\sigma(Z) = 0.18$ and the TOF resolution of σ(TOF) = 100 ps were sufficient to unambiguously identify A and Z for each fragment. The contamination from neighboring isotopes was less than 0.1 %.

It is crucial for any transmission measurement to accurately count all non-interacting particles downstream from the F2 reaction target. For our experimental setup (see Fig. 1) this requires the transmission between the F2 and F4 focal planes to be the same for the measurements with and without F2 target. In order to control the divergence of the secondary beams which might cause particle losses due to the limited geometrical acceptance of the FRS ($\epsilon_{x(y)} = 20\,\pi$mm mrad, $\frac{\Delta p}{p} = \pm 1$ % [18]), two fast multiwire proportional chambers (MWPC) with single wire readout were placed in front of the F2 target. These chambers can be operated with a beam intensity of up to 5×10^5 ions per second. Ray-tracing of the beam particles enabled us to cut the beam emittance in an offline analysis and to guarantee full transmission. The details of the offline analysis are discussed in Section 3.

An additional carbon target placed at F4, combined with a ΔE - TOF measurement based on the scintillators SC41, SC42 and SC43 (see Fig. 1), enabled us to obtain nuclear charge-changing cross-sections for the fragmentation of the secondary beams.

3 Interaction cross-sections

The σ_I values have been derived from measurements performed with and without F2 target:

$$\sigma_I = \frac{1}{t} \log \left(\frac{R_{out}}{R_{in}} \right) \tag{1}$$

where t is the target thickness and $R_{in(out)} = N^{in(out)}/N_o^{in(out)}$ is the ratio of the number of beam particles ($N^{in(out)}$) which passed through the target without interaction, to the number of incident beam particles ($N_o^{in(out)}$), determined with (subscript in) and without (subscript out) target in the beam. There is an additional term

which takes into account the effect of energy loss in the F2 target and the interaction of the beam particles with material located downstream. Since σ_I for relativistic heavy ions is almost independent from the ion energy this term can be neglected.

Systematical uncertainties in the experimental transmission between F2 and F4 arise from the following effects:

- The transmission of the beam particles through the second stage of the FRS was not 100% due to its limited geometrical acceptance. Energy and angular straggling in the target result in different transmissions for the measurement with and without target at F2. The difference in transmission (which has a strong influence on the resulting σ_I) strongly depends on Z and varies from 4% for ^{20}Mg to less than 0.3% for ^{20}N. This effect was taken into account by two methods. Firstly, differences in transmission were calculated by using the Monte-Carlo code MOCADI [19], and the σ_I values were corrected correspondingly. Secondly, a set of position-sensitive fast proportional chambers (MWPC) in front of the F2 target was used to introduce cuts on the angular divergence and momentum spread of the secondary beams. The σ_I values were then determined for different cuts till saturation was reached. Both methods gave the same results within the statistical errors.
- The MUSIC chamber which was used for Z - identification at F4 is a slow device. Its characteristics thus depends on the count rate at F4, which was quite different for the measurements with and without F2 target. Since the F2 target acts as a degrader, the admixture of isotopes with different Z produced in the beryllium target was strongly reduced for the measurements with F2 target. This effect, which is most important for fragments with low production cross-section leads, e.g. for the case of ^{20}N and the thick F2 target, to a 5% decrease of the FWHM of the energy loss measured by the MUSIC. As rather long time gates ($\approx 5\mu$s) were used for the MUSIC chamber there was a non-negligible probability that the MUSIC signal of an ion sums with that of another ion of higher Z. In this case the ADC registered an energy deposition which corresponds to higher Z values. This effect is especially important for low Z isotopes and, in the worst case, accounts for nearly 1.5% of the events measured. To compensate for this specific MUSIC properties, the MUSIC response function was carefully studied for different count rates and for each kind of beam particles using the ΔE - TOF information from the fast scintillation detectors SC41, SC42 and SC43.
- The ions arriving at F2 may induce fragmentation reactions in the target. The fragments with $B\rho$ values close to the one selected can reach the detectors at F4 yielding well separated peaks in the energy loss spectra. The corresponding corrections can easily be introduced. In the case of the thick F2 target, this effect contributed by 0.4 - 0.8% to the F4 count rate.
- Statistical uncertainties were estimated in the following way. In the geometry used in our experiment with fixed numbers of incoming primary fragments N_o^{in} and N_o^{out}, the number of reactions in the target $N_o^{in} - N^{in}$ follows a binomial distribution with the probability of noninteraction $p = N^{in}/N_o^{in}$. The standard deviation

Table 1

Experimental interaction cross-sections σ_I (mb) and deduced rms matter radii (fm) from the present work for different density parametrizations: the modified harmonic-oscillator model (MHO) and the two parameter Fermi model (2pF). Details are given in the text.

Nucleus	σ_I (mb)	rms matter radius (fm)		
		MHO	2pF*	2pF**
^{20}Mg	1150(12)	2.89(3)	2.86(3)	2.86(3)
^{20}Na	1094(11)	2.73(3)	2.69(3)	2.74(3)
^{20}Ne	1144(10)	2.87(3)	2.84(3)	2.85(3)
^{20}F	1113(11)	2.79(3)	2.75(3)	2.78(3)
^{20}O	1078(10)	2.69(3)	2.64(3)	2.70(3)
^{20}N	1121(17)	2.81(4)	2.77(4)	2.80(4)

* the half density parameter r_0 was varied to adjust the calculations to the experimental data
** the surface thickness parameter a was varied to adjust the calculations to the experimental data

in this case is $\delta p = \sqrt{\frac{p(1-p)}{N_o}}$. The statistical uncertainty of σ_I (see formula 1) is thus equal to:

$$\delta\sigma_I = \frac{1}{t}\sqrt{\frac{1-R_{out}}{N_o^{out}R_{out}} + \frac{1-R_{in}}{N_o^{in}R_{in}}} \tag{2}$$

In addition, the above-mentioned effects introduce systematical uncertainties on the level of about 0.8 %.

The resulting σ_I values shown in Fig. 2(a) and Tab. 1 reveal a rather irregular dependence on the isospin projection T_z, which we want to discuss in comparison with results from other experiments. Besides the present measurement several experiments have determined σ_I for the $A = 20$ isobars [20–23], however at different energies and with different target nuclei. A direct comparison with the results of present experiment is therefore not possible. Nevertheless, one can compare the results on the basis of a model parameterization.

The hard-spheres model of "colliding billiard-balls" in which $\sigma_I = \pi R_0^2(A_p^{1/3} + A_t^{1/3})^2$, with A_p and A_t being the mass numbers of projectile and target, reproduces the main properties of high-energy heavy-ion reactions on complex target nuclei. On the other hand, the model is inaccurate in many cases due to the absence of any

energy dependence. The empirical parameterization of σ_I based on the hard-spheres model yields, however, a very good description of the σ_I behavior, if the experimental data are carefully fitted over a wide range of energy and for a variety of colliding systems [24]:

$$\sigma_I = \pi r_0^2 \cdot \left[A_p^{1/3} + A_t^{1/3} + a\frac{A_p^{1/3}A_t^{1/3}}{A_p^{1/3} + A_t^{1/3}} - C(E) \right]^2 \left[1 - \frac{B_c}{E_{cm}} \right] \qquad (3)$$

where a is an asymmetry parameter, $B_c = \frac{Z_p Z_t e^2}{1.3(A_p^{1/3}+A_t^{1/3})}$ is the Coulomb barrier, Z_p and Z_t are the atomic numbers of projectile and target, and $C(E) = 0.31 + 0.0144E/A_p$ for $E \leq 100$·A MeV (1.75 for higher energies) is an energy dependent parameter. It was found that a is independent on the beam energy and projectile-target combination [24] while the strong absorption radius r_0 contains information on the size of the nuclei involved [22].

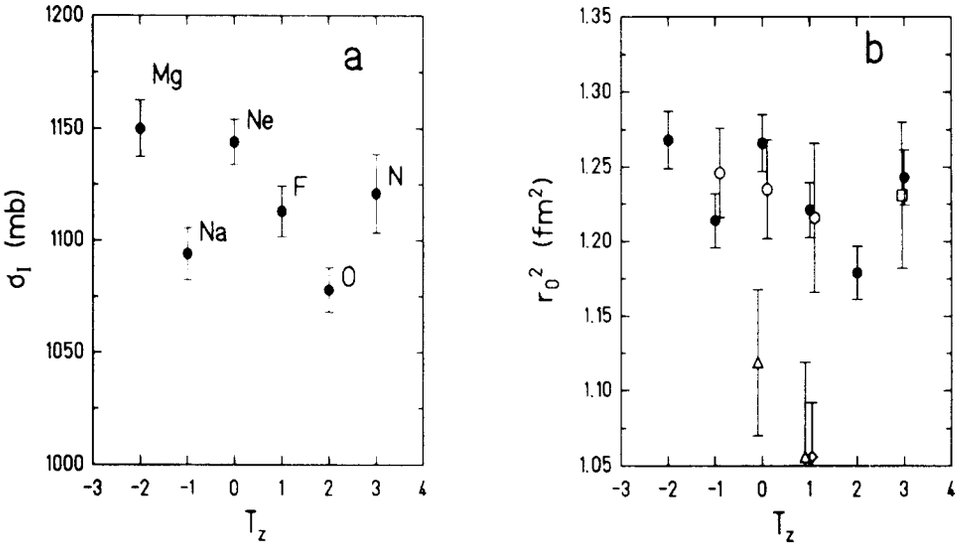

Fig. 2.
(a) Interaction cross-sections measured for $A = 20$ isobars. (b) Comparison of the strong absorption radius parameter r_0^2 for measurements at different incident energies. A normalization was made for ^{20}O. Experimental data from this work at 950 MeV/u are shown by solid circles, open circles indicate data from ref.[20] at 30-60 MeV/u, triangles from ref.[21] at 19-25 MeV/u, squares from ref.[22] at 30-60 MeV/u, and rhombuses from ref.[23] at 40-60 MeV/u.

Equation (3) provides a way to compare the reaction cross-sections at different energies in terms of the r_0 parameter. It is interesting to note the surprisingly linear dependence of r_0 on the neutron excess, which does not depend on the atomic number of nuclei, as has been pointed out in ref. [23]. This result, however, was not con-

firmed by another measurement [21].

Fig.2(b) compares the r_0^2 values for the $A = 20$ isobars obtained from the present experiment with those measured at lower energies. In order to compensate for possible influences of the different target nuclei, a normalization was made for ^{20}O, the only common nucleus in all measurements. As can be seen in Fig.2(b), some of the existing experimental data agree well with the data obtained from present work, while others deviate. Our conclusion is that this discrepancy is due to either experimental problems in the low energy experiments or limits of the simple parametrization shown by equation (3). We shall not discuss this point any further, but shall return to an interpretation of the high-energy σ_I data in Section 5.

4 Charge-changing cross-sections

Nuclear fragmentation in intermediate and high-energy nucleus-nucleus collisions represents a problem of such complexity that the variety of reaction mechanisms is commonly replaced by statistical methods. The fragmentation process is usually described by two-step abrasion-ablation models (see ref.[25] and references therein). In the abrasion stage, the intranuclear cascade or the so called participant-spectator process leads to the removal of nucleons from the projectile. The remaining part of the projectile (prefragment) is excited and undergoes subsequent particle emission in the second (ablation) stage. The mechanism of abrasion determines the nucleon composition of the prefragments and the transferred excitation energy, both parameters influencing drastically the results of the ablation stage. The structure of the projectile (e.g. the proton (neutron) excess at the nuclear surface and nuclear clustering) has been ignored in the description of the first stage. This approximation works well for collisions between heavy nuclei. However, this is not the case for the fragmentation of light nuclei where statistical methods cannot be applied, and both the reaction mechanism and the internal structure of the projectile influence the fragment distributions. For example, the fragmentation of nuclei with a well developed α - cluster structure (^{12}C, ^{16}O, ^{20}Ne) can be successfully described by models based on an α-nucleon interaction (e.g. α - cluster knockout) [26,27]. Moreover, it has been found that nucleon-nucleon correlation effects inside the participating nuclei are far from being negligible [28]. Therefore, one can expect that the special structure of ^{20}Mg may lead to an unusual type of fragmentation reaction.

To study this phenomenon, the charge-changing cross-sections (σ_z) for the $A = 20$ isobars were measured in the present experiment. For this purpose, a carbon target with a thickness of 2.3 g/cm^2 was installed at the F4 focal plane of the FRS. The element composition of the incoming beams was analysed by the method described in Section 2 leading to isotopically clean beams of the desired ions. The fragments resulting from the interaction of these ions with the F4 target were detected in a set of two thin scintillation detectors SC42 and SC43 (see Fig.1) which covered a solid

Table 2

Z - distributions of reaction products from fragmentation of $A = 20$ nuclei.

Projectile fragment	^{20}Mg	^{20}Na	^{20}Ne	^{20}F
reaction products	charge-changing cross sections (mb)			
Na	5(8)	-	-	-
Ne	123(9)	28(8)	-	-
F	29(9)	64(9)	77(7)	-
O	127(7)	127(9)	114(6)	106(8)
N	46(5)	78(8)	96(6)	112(8)
C	146(7)	120(10)	123(6)	104(8)

angle large enough to detect the main part of the fragments. The comparison of the energy loss spectra in these two detectors allowed to correct for the nuclear reactions in the detectors itself. A correction for the attenuation of the beam and the secondary fragments inside the target has been included, for the target thickness was $\approx 10\,\%$ of the beam particles mean free path. Consequently, the expression for the charge-changing cross-section σ_z takes the form:

$$\sigma_z = \frac{N_z}{N_p}\left[\frac{\sigma_I(p) - \sigma_I(z)}{\exp(-\sigma_I(z)\,t) - \exp(-\sigma_I(p)\,t)}\right] \tag{4}$$

where N_z/N_p is the ratio of the number of reaction products to the number of projectiles, t is the target thickness and $\sigma_I(p,z)$ are the σ_I values for projectile and fragments, respectively. The σ_I values were calculated by semiempirical formulae [24]. Since only a correction term is concerned, the sensitivity to uncertainties in σ_I is very low.

The results of the measurements are shown in Tab. 2. A strong enhancement of Ne - and O - isotope yields has been observed in the fragmentation of ^{20}Mg and ^{20}Na nuclei. The distributions cannot be described by phenomenological partial cross-section formulae [29]. Qualitatively, such a behavior can be explained by a combination of valence proton correlations and an α - cluster structure in the core of the incident nuclei. An isotope identification of the fragments produced is necessary to make a final conclusion whether the enhancement observed is indeed connected with the internal structure of the fragmenting nuclei.

5 Interaction cross-sections and nuclear radii

The σ_I data obtained in the present experiment have been analysed in the optical limit of the Glauber model [30]. In this model, σ_I can be written as:

$$\sigma_I = \pi \int_0^\infty [1 - T(r)]\, r dr \tag{5}$$

where $T(r)$ is the transmission function for the impact parameter r. $T(r)$ was calculated as the integral over an overlapping volume of colliding nuclei with the known density distributions $f_{P(T)}(\vec{r})$, using total free nucleon-nucleon cross-sections $\sigma_{i,j}$ (i, j refer to protons and neutrons, respectively) taken from ref. [32]:

$$T(r) = exp\left[-\sum_{i,j=1}^{2} \sigma_{i,j} \int_{-\infty}^{\infty} \rho_{T,i}(r,z)\rho_{P,j}(r,z)dz\right] \tag{6}$$

$$\rho_{T,i}(r,z)\rho_{P,j}(r,z) = 2\pi \int_{-\infty}^{\infty} d\eta \int_0^\infty f_{T,i}(\eta^2 + b^2) \cdot f_{P,j}([(r^2+z^2)^{1/2} - \eta]^2 + b^2) b db \tag{7}$$

Two types of density distributions have been used in the present analysis:

- the modified harmonic-oscillator model (MHO):

$$f(r) = \rho_0(1 + \alpha(r/a)^2)\exp(-r^2/a^2) \tag{8}$$

- the two parameter Fermi model (2pF):

$$f(r) = \rho_0/(1 + \exp((r_0 - r)/a)) \tag{9}$$

The parameters of the MHO density distribution for the ^{12}C target nuclei were taken from electron scattering data [36] and were corrected for the finite size of the proton: $a = \sqrt{a_c^2 - a_p^2}$ and $\alpha = \alpha_c a_c^2/(a^2 + \frac{3}{2}\alpha_c a_p^2)$, where $a_p^2 = \frac{2}{3} < r_c^2 >_{proton}$, $< r_c^2 >_{proton}$ is the proton charge radius, and a_c , α_c are the parameters of the charge distribution obtained from ref. [36]. A value of 0.8 fm was used for $< r_c^2 >_{proton}^{1/2}$ (see ref. [37] and references therein). The MHO density distribution was tested by comparison of σ_I values calculated for carbon - on - carbon reactions with experimental data. The result of this comparison is shown in Fig.3(a).

The initial parameters for the projectile density distributions were also taken from electron scattering data. The MHO parameters were adjusted to the measured ^{18}O charge distribution [38], while the 2pF density was assumed to be the same as for the

measured ^{20}Ne charge distribution [38]. In both cases we have corrected the charge density distributions for the finite size of the proton. The Fermi density parameterization after such a correction results in a larger value for the half density parameter r_0 (2.816 fm instead of 2.740 fm as obtained by using data from the electron scattering experiment) and a smaller value for the surface thickness a (0.512 fm instead of 0.572 fm). The quality of the description of existing experimental σ_I data from ^{12}C+^{20}Ne reactions is shown in Fig. 3(b). All calculations in Fig. 3(a,b) were made without any adjustment of the parameters.

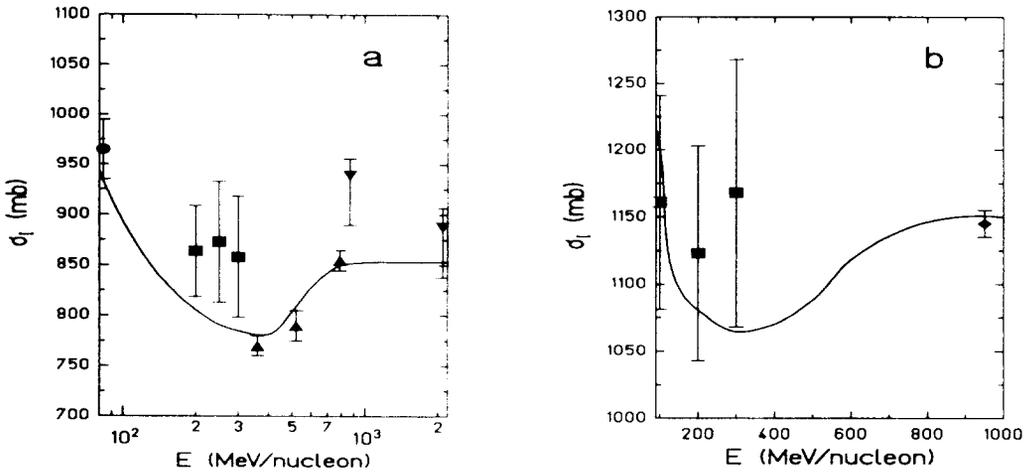

Fig. 3.
Comparison of experimental σ_I for ^{12}C+^{12}C (a) and ^{20}Ne+^{12}C (b) with Glauber type model calculations (solid lines). The experimental data are indicated by circles (ref.[33]), squares (ref.[24]), triangles (ref.[34]), inverse triangles (ref.[35]) and rhombuses (present work). Calculations were done with density distributions taken from electron scattering data [38] without any adjustment of the parameters.

The density distributions (MHO, 2pF) used in the present analysis have two parameters which in principle cannot be determined unambiguously from σ_I measured for one energy. However, the calculations for the MHO densities show that σ_I is mainly determined by the rms matter radius $< r_m^2 >^{1/2}$. This fact is demonstrated in Fig.4(a) where the relation between σ_I and the MHO parameters is shown for the interaction of ^{20}Ne with a ^{12}C target. The rms radius can be unambiguously obtained from σ_I if the curves for constant $< r_m^2 >^{1/2}$ are parallel to those for constant σ_I in the diffuseness parameter (a) *vs.* radius parameter (α, r_0) plane. As can be seen in Fig.4(a), the loci of constant σ_I (dashed curves) are almost parallel to the loci of constant $< r_m^2 >^{1/2}$ (solid curves) and thus give the possibility of rms radius determination from σ_I. The Fermi model (2pF) density distributions with a larger diffuseness results in larger interaction cross-sections as can be seen in Fig. 4(b). As was shown in ref. [39], the optical limit of the Glauber model overestimates the nuclear surface contribution especially for a very diffuse surface. However, the de-

pendence for the 2pF model is still rather weak and within a reasonable range of the diffuseness parameter ($a \approx 0.4 - 0.6$ fm), the $< r_m^2 >^{1/2}$ can be determined with an accuracy of a few percent. Moreover, Figs. 4(a,b) demonstrate that calculations with a definite value of σ_I result in nearly the same values for the $< r_m^2 >^{1/2}$ for both the MHO and the 2pF density distributions.

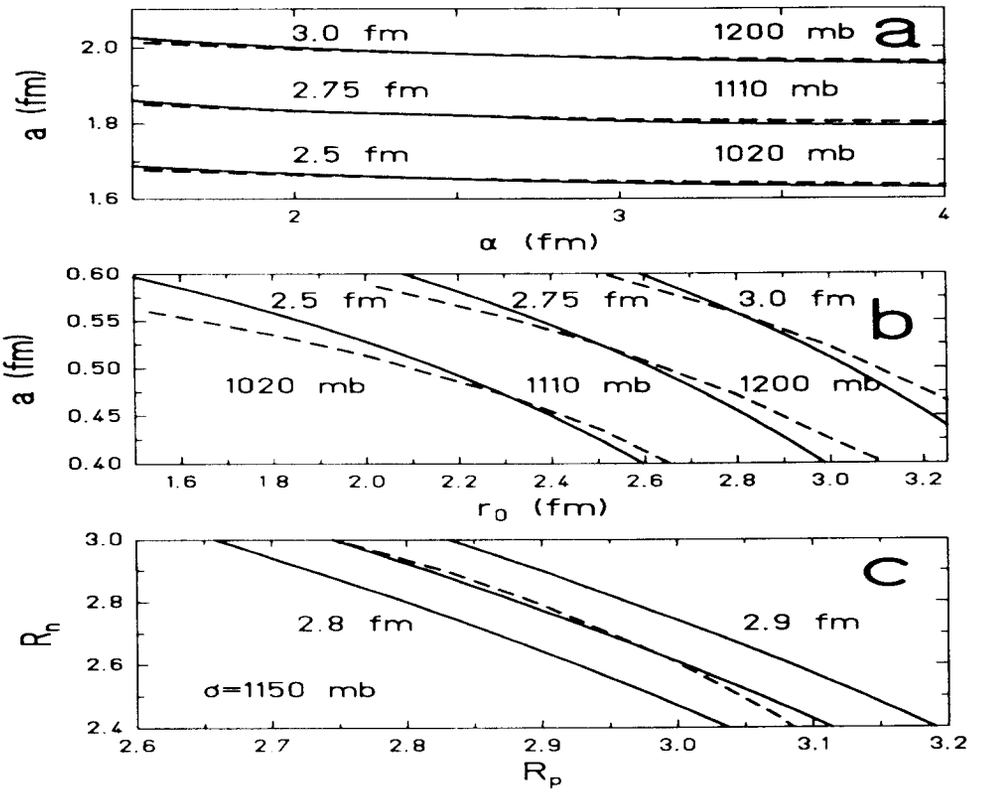

Fig. 4.

Relation between fixed values of σ_I (dashed curves) or projectile rms radii $< r_m^2 >^{1/2}$ (solid curves) and the parameters of the nuclear density distributions. Fig. 4(a,b) show this relation for the MHO parameters a, α and the 2pF parameters a, r_0, for the system ^{20}Ne+^{12}C, respectively. The plotted numbers indicate the values of rms radii and σ_I chosen for the calculations. In (c), the sensitivity of the $\sigma_I - < r_m^2 >^{1/2}$ relation on differences between the neutron (R_n) and the proton (R_p) rms radii is shown for the ^{20}Mg+^{12}C case. The details are explained in the text.

Another problem in the calculations is connected with the different density distributions of neutrons and protons in nuclei. This difference may also result in an ambiguity in the rms matter radii obtained from σ_I. However, Fig.4(c) demonstrates that σ_I again is mainly determined by the $< r_m^2 >^{1/2}$ and only slightly influenced by the differences in neutron and proton rms radii when these are very large.

It is worthwhile to note that the calculations can be considerably simplified by the method using surface-normalized Gaussian distributions [30]. However, when this

method is applied, the calculations show a change in sign for the dependence of the diffuseness parameter on the rms radius; larger cross-sections correspond then to smaller diffuseness. Thus, it is not possible to use this approximation in our case.

Our considerations so far lead us to the conclusion that the main free parameter of the model is $< r_m^2 >^{1/2}$ and that a fit of the measured σ_I values will provide, within the restrictions discussed above, the rms matter radius of the projectile.

6 Discussion

The rms matter radii of the $A = 20$ isobaric sequence have been derived from the experimental σ_I values for two different density parametrizations, MHO and 2pF. For the Fermi model density (2pF), two cases were considered:
(1) the half density parameter r_0 was varied to fit the experimental data while the surface thickness parameter a was kept constant,
(2) a was varied while r_0 was kept constant.
As can be seen from Tab. 1, the values obtained for the rms matter radii in these two extrem cases agree well within the uncertainties of σ_I which are entirely due to statistical and systematical uncertainties from the experiment (see Section 3); the model descriptions were assumed to be exact in this context.

The dependence of nuclear matter radii on the isospin projection T_z obtained from the present analysis (see Fig.5(a) and Tab. 1) is surprising at first sight. The nucleus ^{20}Ne, which is known to be strongly deformed, reveals a relatively large $< r_m^2 >^{1/2}$. ^{20}O with a magic number of protons has the smallest radius of all nuclei investigated. Its radius is smaller by 0.2 fm than the radius of the mirror nucleus ^{20}Mg. This is probably related to a difference in binding energies of these nuclei, and gives some evidence for the existence of a proton skin in ^{20}Mg. The $< r_m^2 >^{1/2}$ of the two other mirror nuclei, ^{20}F and ^{20}Na, are equal within the experimental errors.

In Fig.5(a), the experimental data from the present work are compared with the results of relativistic mean-field (RMF) calculations (solid line), which include shell effects and deformation. The irregular dependence of the $< r_m^2 >^{1/2}$ on T_z observed experimentally is qualitatively reproduced. As will be discussed below, the RMF model parameters were adjusted to reproduce the rms charge radii $< r_c^2 >^{1/2}$ but not $< r_m^2 >^{1/2}$. In these calculations, the potentials were determined by using the parameter set NL2 [43,44]. These parameters were adjusted in such a way that the model reproduces measured ground state properties of nuclei such as charge radii and charge density distributions as good as possible. The set NL2 is found to describe well the charge radii in the entire $2s1d$ - shell region [44,45].

Before we compare the predictions of RMF for the $< r_c^2 >^{1/2}$ of the $A = 20$ nuclei to experimental results, it is worthwhile to note that the nuclear charge radii

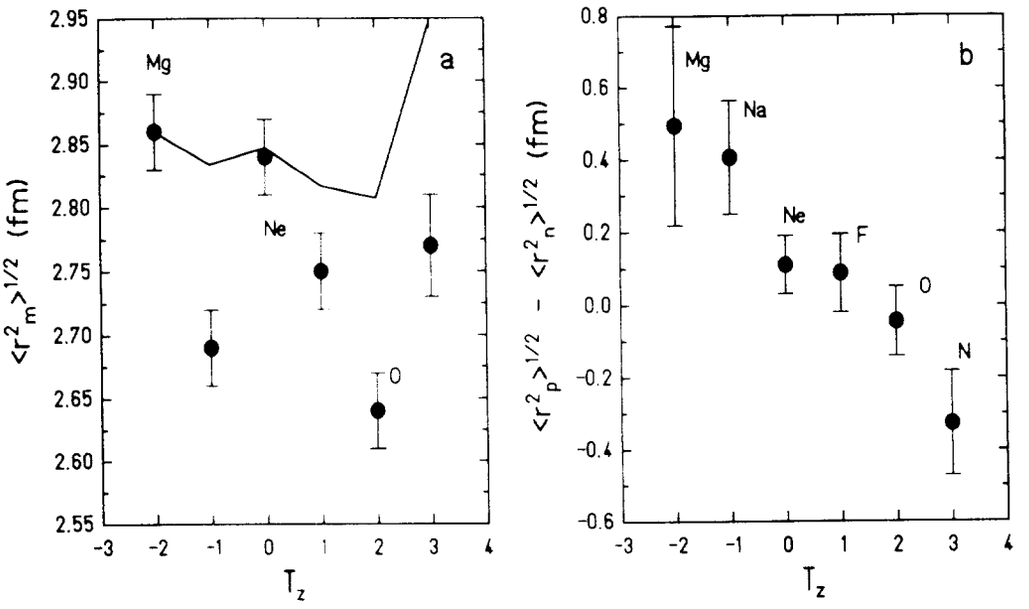

Fig. 5.

(a) Dependence of rms matter radii on the isospin projection T_z for $A = 20$ isobars. The solid line represents the result of a relativistic mean-field calculation. (b) Difference between neutron and proton radii for the $A = 20$ isobaric sequence.

for the *sd* - shell nuclei, which depend on the proton distributions (in contrast to the matter radii discussed so far), behave anomalously as well. Fig. 6 demonstrates this irregular behavior for stable nuclei as function of the atomic mass number A. The $< r_c^2 >^{1/2}$ of the even-even nuclei with $N = Z$ are systematically larger than those of neighboring nuclei. Since their charge form factors can be reproduced in α - cluster models which include short range nucleon-nucleon correlations [41], the observed peculiarities are most likely connected with the α - cluster structure of these nuclei (see ref. [40] and references therein). It is interesting to note that the addition of a neutron to such a nucleus results in a more compact configuration. The values of $< r_c^2 >^{1/2}$ in Fig.6 have been obtained either from electron scattering experiments [38] or from X - ray measurements on muonic atoms (the latter we use for further discussion) [16].

The difference between the charge radii, $\Delta r_c = < r_c^2(A+2) >^{1/2} - < r_c^2(A) >^{1/2}$ of ^{18}O and ^{16}O is larger than any other such difference between two neighboring even-even isotopes measured so far. Furthermore, the Δr_c difference between ^{22}Ne and ^{20}Ne turns out to be more negative than the most negative Δr_c data of neighboring even-even isotopes. Such a decrease may be related to a decrease in intrinsic nuclear deformation. An unusually large value for Δr_c is observed between ^{18}O and ^{20}Ne, whereas a very small value is found between ^{22}Ne and ^{24}Mg (compare Fig.6).

We now compare the rms charge radii for the $A = 20$ isobars as derived from the

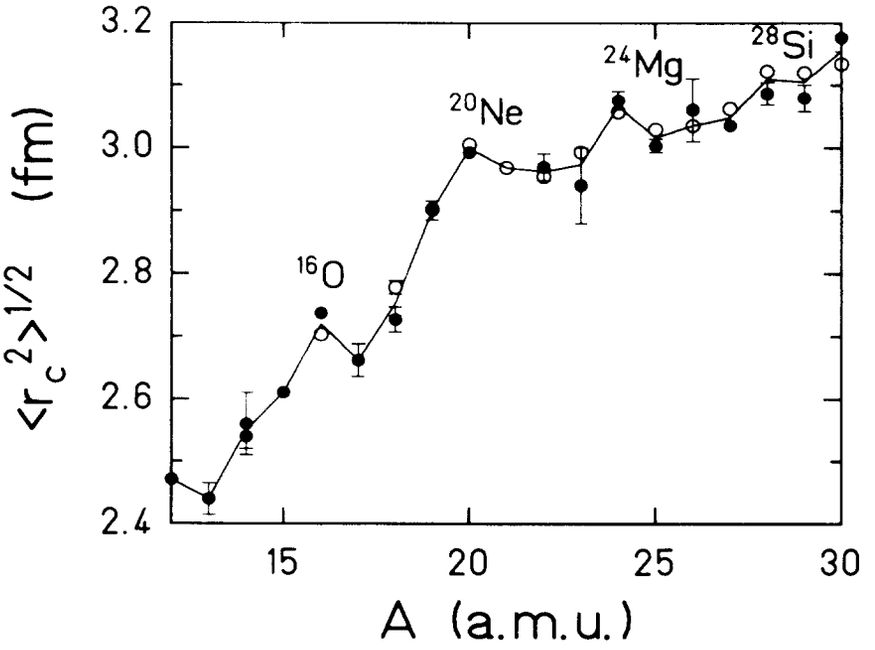

Fig. 6.
Dependence of charge radii $< r_c^2 >^{1/2}$ for stable *sd* - shell nuclei on the mass number A. Solid circles represent data obtained from electron scattering [38], open circles show results from muonic-atom experiments [16].

RMF calculations using the NL2 parameter set with values based on existing experimental data. The results are summarized in Fig. 7. The charge radius $< r_c^2 >^{1/2}$ of ^{20}Ne is known e.g. from X - ray measurements of muonic atoms [16]. Isotope shift measurements [48] allow to evaluate the $< r_c^2 >^{1/2}$ of ^{20}Na by using a semiempirical model and taking the charge radius of ^{23}Na [16] as a reference. Unfortunately, the result is extremely sensitive to the mass shift parameter and model dependent in this way. The uncertainty in the $< r_p^2 >^{1/2}$ (see below) of ^{20}Na indicated in Fig. 7 was obtained by changing the model parameters within a reasonable range. Finally, the $< r_c^2 >^{1/2}$ of ^{20}O and ^{20}F can be evaluated by extrapolation from the known radii of ^{17,18}O and ^{19}F [16,38]. In this case, we used the fact that the Coulomb displacement energies (ΔE_c) of isotopic sequences (O - F and F - Ne) are inversely proportional to the charge radii [49]. A comparison of ΔE_c values for isotopes with experimentally known charge radii (oxygen, magnesium, potassium, calcium) shows that this statement is valid within 2% of the accuracy in radii. Finally, the value for $< r_c^2 >^{1/2}$ of ^{20}Mg can be evaluated by linear extrapolation [15] from radii of ^{24,25,26}Mg [16]. The radii obtained by these methods are in good agreement with the RMF calculations as can be seen from Fig. 7.

The rms radii of the proton distributions, $< r_p^2 >=< r_c^2 > - < r_c^2 >_{proton}$, that are displayed in Fig. 7 as results from experiment or from empirical extrapolations, and

the experimental $< r_m^2 >^{1/2}$ values obtained in this work were used to derive the differences between the radii of neutron and proton distributions. These differences are shown in Fig. 5(b). For all isobars except ^{20}Mg, ^{20}Na, and ^{20}N the resulting differences disappear within the experimental uncertainties. However, the difference is significant for those nuclei with a large excess of neutrons (^{20}N) or protons (^{20}Mg, ^{20}Na). The thickness of the proton skin for ^{20}Mg ($\approx$ 0.5 fm) is about the same as the thickness of the neutron skin in the ^{20}N case.

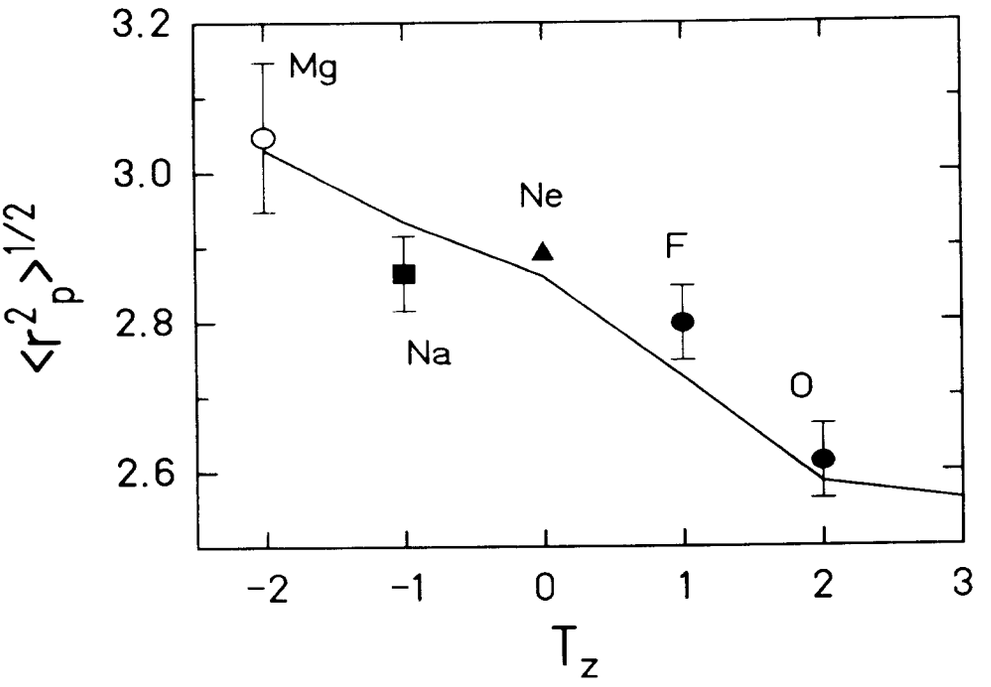

Fig. 7.
Rms radii of proton density distributions of $A = 20$ isobars. The values for ^{20}O and ^{20}F, obtained by extrapolation from the known radii of ^{17,18}O and ^{19}F [16,38] are shown by solid circles. The result of a linear extrapolation from known radii of the ^{24,25,26}Mg isotopes to ^{20}Mg is indicated by an open circle. The triangle represents the radius of ^{20}Ne [16]. The radius of ^{20}Na as estimated from isotope shift measurements [47] is shown by the square. The solid line represents the result of a RMF calculation.

As was already mentioned in Section 1, a study of matter radii in the $A = 17$ sequence [7] revealed an anomalously large value for the proton-rich ^{17}Ne isotope. The proton halo of ^{17}Ne, which has been obtained from these data, was interpreted by demanding the last two protons in this nucleus to be abnormally in a $2s_{1/2}$ orbital [7,8]. One would expect the Coulomb displacement energies to reflect such an admixture if this effect influences the radii. However, the comparison of Coulomb displacement energies for the members of the T=2 multiplet (^{20}O - ^{20}F) with those of

the T=1/2 nuclei (^{17}O - ^{17}F) in $2s_{1/2}$ and $1d_{5/2}$ states does not show any significant influence of a possible admixture of a $2s$ state in the T=2 multiplet. Hence, this effect alone cannot explain the large radius of ^{20}Mg [42]. Moreover, the dependence of Coulomb displacement energies of the T=2 multiplet members on Z observed experimentally is contradictory to the behavior expected from the uniform charge spheres model. Good agreement with this ΔE_c dependence can be achieved indeed, when a strong correlation between the valence protons of the nuclei under investigation is included in the calculations. Evidence for valence proton correlations was also found from considering the proton binding energies for the systems of ^{16}O plus a few protons [42]. This observation lead to the conclusion that ^{20}Mg has a very specific structure characterized by a ^{16}O core and a four-proton cluster. For ^{20}Mg, not the admixture of low orbital momentum states (as for the ^{17}Ne case), but correlations between the valence protons, arising from their mutual interaction, determine the existence of a proton skin. This skin is not a uniform proton distribution around the core nucleus, but a specific cluster-like structure due to strong correlations between the valence protons [42]. By this means, the large radius of ^{20}Mg has the same origin as the large charge radii of titanium isotopes in comparison to their calcium isobars, as discussed in Section 1, or the neutron skin of ^{18}O and the proton skin of ^{18}Ne predicted theoretically [31].

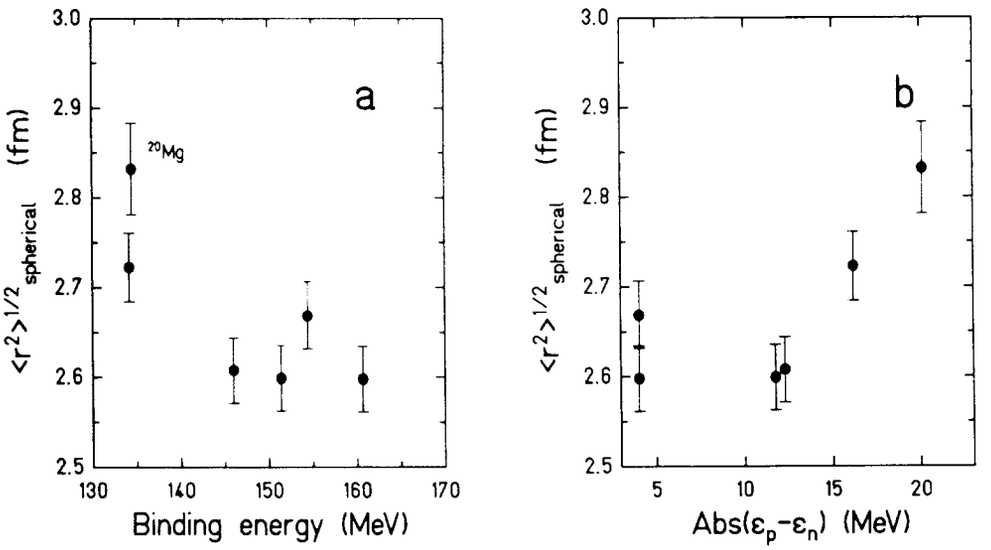

Fig. 8.
(a) Dependence of the "spherical part" (see text) of the rms matter radii on binding energy for $A = 20$ isobars. (b) Dependence of the "spherical part" of rms matter radii on the difference between minimal energies necessary to remove one proton or neutron from a nucleus of the $A = 20$ isobaric sequence.

From an investigation of experimental data around closed-shell nuclei a linear relationship between Δr_c^2 and the binding energies per nucleon $\Delta B/A$ has been found

[11,12]. According to this relationship nuclear radii increase with decreasing binding energy. However, this simple dependence has only a very limited validity. When a more complete basis of accurate measurements of radii is considered, no direct correlation between $\Delta B/A$ and Δr_c^2 can be found with statistical significance. The occurance of shell effects and deformation superimposes fluctuations on top of a smooth global behavior [15], and the relationship can be very complicated. In order to search for the appearance of such a correlation in matter radii for the $A = 20$ isobars, we corrected the measured rms radii for deformation. We follow the procedure described in ref. [16], which is based on a "pairing - plus - quadrupole" model [13], where the nuclear shapes are parametrized as rotational ellipsoids with the deformation being limited to the quadrupole contribution. Under this assumption, the rms radii can be written as:

$$< r^2 >=< r^2 >_{spherical} \left[1 + \frac{5}{4\pi} < \beta_2^2 >\right] \tag{10}$$

The deformation parameters $< \beta_2^2 >$ of the nuclei under consideration were taken from a compilation of experimental data [46] and from RMF calculations.

The common tendency of increasing "spherical" nuclear radii $< r^2 >_{spherical}$ with decreasing binding energy B is visible in Fig. 8(a). This correlation becomes much more pronounced if, instead of B, the differences between the minimal separation energies for neutrons or protons, $\epsilon_p - \epsilon_n$, is used as shown in Fig. 8(b). This fact can be explained by a model in which only the valence nucleons are responsible for the changes in nuclear radii.

7 Summary

Interaction cross-sections for the $A = 20$ isobars ^{20}N, ^{20}O, ^{20}F, ^{20}Ne, ^{20}Na and ^{20}Mg with carbon have been measured within an accuracy of about 1%. Nuclear matter rms radii have been derived from the measured σ_I. A large difference in $< r_m^2 >^{1/2}$ (≈ 0.2 fm) has been obtained for the two mirror nuclei ^{20}O and ^{20}Mg. It was shown that the values of $< r_m^2 >^{1/2}$ are influenced both by nuclear deformation and nuclear binding energy. Evidence has been found that the valence nucleons determine the changes in $< r_m^2 >^{1/2}$.

The differences in rms radii of neutron and proton distributions have been estimated by using $< r_m^2 >^{1/2}$ from the present experiment and charge radii obtained either experimentally or in evaluations based on existing experimental data. The derived charge radii are in good agreement with those calculated by means of RMF theory. A significant difference in radii of neutron and proton distributions (≈ 0.5 fm) has been found for nuclei with a large excess of neutrons (^{20}N) or protons (^{20}Mg, ^{20}Na).

We would like to thank the SIS staff members for their untiring effort to produce high intensity Ar-beams and K.H. Behr, A. Brünle, and K. Burkard for their technical assistance at the FRS. The authors would also like to acknowledge support from DFG and WTZ.

References

[1] I.Tanihata, Prog. Part. Nucl. Phys., 35 (1995) 505

[2] P.G.Hansen, A.S.Jensen, B.Jonson, Preprint Chalmers University, CTHSP-95/05, 1995, Ann. Rev. of Nucl. Part. Science, 45 (1995) in print

[3] J.P.Auger, R.J.Lombard, Phys. Lett. 90 B (1980) 200

[4] Yu.P.Gangrski, S.G.Zemlyanoi, V.I.Zhemenik, K.P.Marinova, B.N.Markov, L.M.Melnikova, JINR Rapid Communications 6[69]-94, Dubna, 1994

[5] R.E.Warner, J.H.Kelley, P.Zecher, F.D.Becchetti, J.A.Brown, C.L.Carpenter, A.Galonsky, J.Kruse, A.Muthukrishnan, A.Nadasen, R.M.Ronningen, P.Schwandt, B.M.Sherrill, J.Wang, J.S.Winfield, Phys. Rev. C 52 (1995) R1166

[6] W.Schwab, H.Geissel, H.Lenske, K.-H.Behr, A.Brünle, K.Burkard, H.Irnich, T.Kobayashi, G.Kraus, A.Magel, G.Münzenberg, F.Nickel, K.Riisager, C.Scheidenberger, B.M.Sherrill, T.Suzuki, B.Voss, Z. Phys. A 350 (1995) 283

[7] A.Ozawa, T.Kobayashi, H.Sato, D.Hirata, I.Tanihata, O.Yamakawa, K.Omata, K.Sugimoto, D.Olson, W.Christie, H.Wieman, Phys.Lett. 334 B (1994) 18

[8] M.V.Zhukov, B.Jonson, Preprint Chalmers University, CTHSP-95/05 1995; Nucl. Phys. (1995) in press

[9] E.Friedman, H.J.Gils, H.Rebel, Phys.Rev. C 25 (1982) 1551

[10] I.Tanihata, T.Kobayashi, T.Suzuki, K.Yoshida, S.Shimoura, K.Sugimoto, K.Matsuta, T.Minamisono, W.Christie, D.Olson, H.Wieman, Phys. Lett. 287 B (1992) 307

[11] S.Gerstenkorn, C.R. Acad.Sci.Ser. B 268 (1969) 1636

[12] R.Wenz, E.Matthias, H.Rinneberg, F.Schneider, Z. Phys. A 295 (1980) 303

[13] B.S.Reehal, R.A.Sorensen, Nucl. Phys. A 161 (1971) 385

[14] F.Barranco, R.A.Broglia, Phys. Lett. 151 B (1985) 90

[15] I.Angeli, R.J.Lombard, Z. Phys. A 324 (1986) 299

[16] G.Fricke, J.Herberz, Th.Hennemann, G.Mallot, L.A.Schaller, L.Schellenberg, C.Piller, R.Jacot-Guillarmod, Phys. Rev. C 45 (1992) 80

[17] T.Suzuki, H.Geissel, O.Bochkarev, L.Chulkov, M.Golovkov, D.Hirata, H.Irnich, Z.Janas, H.Keller, T.Kobayashi, G.Kraus, G.Münzenberg, S.Neumaier, F.Nickel, A.Ozawa, A.Piechaczeck, E.Roeckl, W.Schwab, K.Sümmerer, K.Yoshida, I.Tanihata, Preprint RIKEN-AF-NP-204, 1995 and Rhys. Rev. Lett. 75 (1995) 3241

[18] H.Geissel, P.Armbruster, K.H.Behr, A.Brunle, K.Burkard, M.Chen, H.Folger, B.Franczak, H.Keller, O.Klepper, B.Langenbeck, F.Nickel, E.Pfeng, M.Pfutzner, E.Roeckl, K.Rykaczewski, I.Schall, D.Schardt, C.Scheidenberger, K.-H.Schmidt, A.Schroeter, T.Schwab, K.Sümmerer, M.Weber, G.Münzenberg, T.Brohm, H.-G.Clerc, M.Fauerbach, J.-J.Gaimard, A.Grewe, E.Hanelt, B.Knodler, M.Steiner, B.Voss, J.Weckenmann, C.Ziegler, A.Magel, H.Wollnik, J.P.Dufour, Y.Fujita, D.J.Vieira, B.Sherrill, Nucl. Instr. Meth. in Phys. Res. B 70 (1992) 286

[19] Th.Schwab, Doktorarbeit, Universität Giessen, GSI report 91-10 (1991)

[20] A.C.C.Villari et al., Proc. XXVII Intern. Winter Meeting on Nuclear Physics, Bormio, Italy, 1989, p.24

[21] M.G.Saint-Laurent, R.Anne, D.Bazin, D.Guillemaud-Mueller, U.Jahnke, Jin Gen-Ming, A.C.Mueller, J.F.Bruandet, F.Glasser, S.Kox,E.Liatard, Tsan Ung Chan, G.J. Costa, C.Heitz, Y.El-Masri, F.Hanappe, R.Bimbot, E.Arnold, R.Neugart, Z.Phys. A 332 (1989) 457

[22] A.C.C.Villari, W.Mittig, E.Plagnol, Y.Schutz, M.Lewitowicz, L.Bianchi, B.Fernandez, J.Gastebois, A.Gillibert, C.Stephan, L.Tassan-Got, G.Audi, W.Zhan, A.Cunsolo, A.Foti, A.Belezyorov, S.Lukyanov, Y.Penionzhkevich, Phys. Lett. 268 B (1991) 345

[23] W.Mittig, J.M.Chouvel, Zhan Wen Long, L.Bianchi, A.Cunsolo, B.Fernandez, A.Foti, J.Gastebois, A.Gillibert, C.Gregoire, Y.Schutz, C.Stephan, Phys.Rev.Lett. 59 (1987) 1889

[24] S.Kox, A.Gamp, C.Perrin, J.Arvieux, R.Bertholet, J.F.Bruandet, M.Buenerd, R.Cherkaoui, A.J.Cole, Y.El-Masri, N.Longequeue, J.Menet, F.Merchez, J.B.Viano, Phys. Rev. C 35 (1987) 1678

[25] T.Brohm, K.-H.Schmidt, Nucl. Phys. A 569 (1994) 821

[26] F.A.Cucinotta, R.R.Dubey, Phys.Rev. C 50 (1994) 1090

[27] G.Fäld, L.Gislen, Nucl. Phys., A 254 (1975) 341

[28] T.Kodama, S.B.Duarte, K.C.Chung, R.A.M.S.Nazareth, Phys. Rev. Lett. 49 (1982) 536

[29] K.Sümmerer, W.Brüchle, D.J.Morrissey, M.Schädel, B.Szweryn, W.Yang, Phys. Rev. C 42 (1990) 2546

[30] P.J.Karol, Phys. Rev. C 11 (1975) 1203

[31] M.V.Zhukov, D.H.Feng, Cheng-li Wu, J.Bang, Phys. Scr. 22 (1980) 426 M.V.Zhukov, J.M.G.Gomez, J.Bang, Phys. Scr. 25 (1982) 522

[32] L.Ray, Phys. Rev. C 20 (1979) 1857

[33] C.Perrin, S.Kox, N.Longequeue, J.B.Viano, M.Buenerd, R.Cherkaoui, A.J.Cole, A.Gamp, J.Menet, R.Ost, R.Bertholet, C.Guet, J.Pinston, Phys. Rev. Lett. 49 (1982) 1905

[34] S. Shimoura, I. Tanihata, T. Kobayashi, K. Matsuta, K. Katori, K. Sugimoto, D.L. Olson, W.F.J. Mueller, H.H. Wieman, Proc. of the First Int. Conf. on Radioactive Nuclear Beams, Eds. W.D. Myers, J.M. Nitschke, and E.B. Norman, World Scientific, 1989, p. 439.

[35] J.Jaros, A.Wagner, L.Anderson, O.Chamberlain, R.Z.Fuzesy, J.Gallup, W.Gorn, L.Schroeder, S.Shannon, G.Shapiro, H.Steiner, Phys. Rev. C 18 (1978) 2273

[36] J.A.Jansen, R.T.Peerdeman, C.de Vries, Nucl. Phys. A 188 (1972) 337

[37] M.McCord, H.Crannell, L.W.Fagg, J.T.O'Brien, D.I.Sober, J.W.Lightbody, X.K.Maruyama, P.A.Treado, Nucl. Instr. Meth. in Phys. Res. B 56/57 (1991) 496

[38] H. de Vries, C.W.de Jager, C. de Vries, Atomic Data and Nucl. Data Tables 36 (1987) 495

[39] N.Takigawa, M.Ueda, M.Kuratani, H.Sagawa, Phys. Lett. 288 B (1992) 244

[40] J.Zhang, W.D.M.Rae, Nucl. Phys. A 564 (1993) 252

[41] R.I.Dzhibuti, R.Y.Kezerashvili, Yad.Fiz. 20 (1974) 340; Sov. J. Nucl. Phys. 20 (1975) 181

[42] L.Chulkov, E.Roeckl, G.Kraus, Preprint GSI-95-51 (1995), Z. Phys. A, in print

[43] S.-J.Lee, J.Fink, A.B.Balantekin, M.R.Strayer, A.S.Umar, P.-G.Reinhard, J.A.Maruhn, W.Greiner, Phys. Rev. Lett. 57 (1986) 2916 ; Erratum Phys. Rev. Lett. 59 (1987) 1171

[44] Y.K.Gambhir, P.Ring, A.Thimet, Ann. Phys. 198 (1990) 132

[45] S.K.Patra, Nucl. Phys. A 559 (1993) 173

[46] S.Raman, C.H.Malarkey, W.T.Milner, C.W.Nestor, Jr., P.H.Stelson, At. Data Nucl. Data Tables 36 (1987) 1

[47] F.Touchard, J.M.Serre, S.Buttgenbach, P.Guimbal, R.Klapisch, M.de Saint Simon, C.Thibault, H.T.Duong, P.Juncar, S.Liberman, J.Pinard, J.L.Vialle, Phys. Rev. C 25 (1982) 2756

[48] E.W.Otten, Treatise on heavy ion science, 8 (1989) 517

[49] J.A.Nolen, J.P.Schiffer, Ann. Rev. of Nucl. Sci. 19 (1969) 471